THE JOURNAL OF PHYSICAL CHEMISTRY B

Article

pubs.acs.org/JPCB

Measuring the Spatial Distribution of Dielectric Constants in Polymers through Quasi-Single Molecule Microscopy

Chelsea M. Hess, Erin A. Riley, Jorge Palos-Chávez, and Philip J. Reid*

Department of Chemistry, University of Washington, Box 351700, Seattle, Washington 98195, United States

Supporting Information

ABSTRACT: The variation in dielectric constant is measured for thin films of poly(methyl methacrylate) (PMMA) and poly(vinylidene fluoride) (PVDF) using confocal fluorescence microscopy. Spatial variation in the local dielectric constant of the polymer films on the ∼250 nm length scale is measured using the solvochromatic emission from incorporated nile red (NR) at "quasi-single molecule" (10^{-7} M) and true single molecule (SM) concentrations (10^{-9} M). Correlation of the NR fluorescence wavelength maximum with dielectric constant is used to transform images of NR's emission maxima to spatial variation in local dielectric constant. We demonstrate that the distributions of dielectric environments measured in the quasi- and true SM approaches are equivalent; however, the enhanced signal rates present in the quasi-SM approach result in this technique being more efficient. In addition, the quasi-SM technique reports directly on the continuous spatial variation in dielectric constant, information that is difficult to obtain in true SM studies. With regards to the polymers of interest, the results presented here demonstrate that a limited distribution of dielectric environments is present in PMMA; however, a broad distribution of environments exists in PVDF consistent with this polymer existing as a distribution of structural phases.

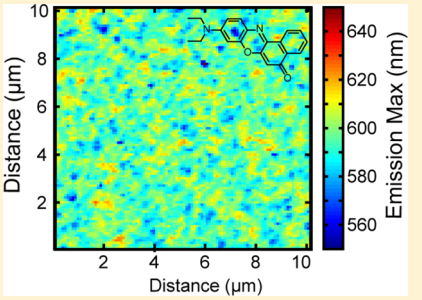

INTRODUCTION

Measuring the distribution of dielectric environments at the nanoscale is an emerging area of interest.[1−3] Largely motivated by the development of new materials such as nanopatterned dielectrics, knowledge of the spatial distribution of dielectric constants (ε) is requisite in describing the properties of these materials. Our group is particularly interested in the dielectric properties of polymers used in electro-optical (EO) devices. Recent studies demonstrated a 2-fold increase in the hyperpolarizability of EO chromophores with an increase in ε from 2 to 36.[4] Given the dependence of EO activity on ε, knowledge of the distribution of ε within the polymer host is fundamental for predicting the EO activity of guest chromophores and overall material performance.

Measurements of ε for polymer films as thin as 5 nm can be performed using broad-band dielectric spectroscopy; however, this technique has limited spatial resolution.[5] Recently, measurements of ε on nanometer length scales have been performed using nanoscale dielectric microscopy.[1] This technique employs a nanoscale capacitance microscope (NCM) corresponding to a modified atomic force microscope (AFM) equipped with a low frequency alternating current detection system. The NCM acquires two scans of the sample: one scan measuring film thickness and the other measuring ε through a subattofarad capacitance detector. A significant limitation of this technique is that film thickness must be <20 nm. Another promising technique for measuring the dielectric properties of polymers is frequency modulation electrostatic force microscopy (fm-EFM).[3,6] Although this method does not directly measure ε, it does provide a measure of the dielectric response with ∼40-nm spatial resolution. Finally, it should be noted that both NCM and fm-EFM techniques are surface measurement.

Approaches for measuring distributions of ε in polymers generally employ solvatochromic dyes serving as nanoreporters of the local environment. Nile red (NR) has been widely used for this purpose, with the solvatochromic properties of this dye illustrated in Figure 1. The emission from NR exhibits a ∼100 nm bathochromic shift with a change in ε from ∼2 to ∼32.[7−10]

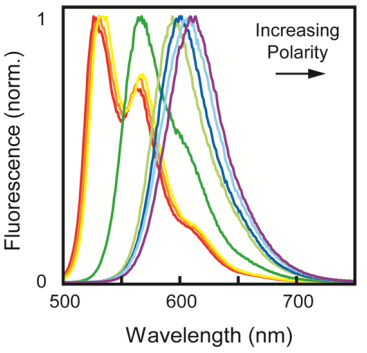

Figure 1. Fluorescence spectra of NR in hexane (red), heptane (orange), cyclohexane (yellow), toluene (dark green), chloroform (light green), dichloromethane (dark blue), acetone (light blue), and acetonitrile (dark purple) obtained with a 488-nm excitation.

Received: January 24, 2013
Revised: May 14, 2013

   dx.doi.org/10.1021/jp4008398 | J. Phys. Chem. B XXXX, XXX, XXX−XXX

The figure demonstrates that changes in the NR emission line shape are also observed between nonpolar (cyclohexane, heptane, and hexane) and polar solvents. These changes have been attributed to specific solvent interactions such as dipole−dipole, which increase the homogeneous line width.[7,11] NR has previously been used to measure the evolution in ε for poly(vinylidene fluoride) (PVDF) films accompanying the transition from disordered α phase to ferroelectric β phase upon stretching.[12] NR has also been used in single-molecule (SM) studies of dielectric heterogeneity in poly(methyl methacrylate) (PMMA) and poly(vinyl alcohol).[9] Although informative, SM studies involve the measurement of many individual molecules to achieve a statistically significant measure of the distribution of ε such that this approach can be time-consuming. In addition, information regarding the spatial variation in ε is extremely difficult to obtain using SM approaches.

We report here a quasi-SM method for measuring the spatial variation of ε in polymer films. Specifically, confocal fluorescence microscopy is used to measure the distribution of ε in PMMA and PVDF films. PMMA is a widely studied polymer[13] with a modest dielectric constant ($\varepsilon \approx 3$).[14] In comparison, PVDF has a range of $\varepsilon \approx 6-13$ for α and β phase films, respectively;[14] and its dielectric, ferroelectric, piezoelectric, and pyroelectric properties have been exploited in innumerable technical applications such as optical devices, sensors, biomedical materials, and fuel cells.[15] The variation in ε for these polymers is determined by measuring solvatochromic shifts of NR emission, which directly report on the local ε of the surroundings. This approach has been employed at the SM level by others;[9] however, in these previous studies, the chromophores were separated by distances of micrometers such that measurement of the spatial variation in ε was not possible. In this study, NR concentrations roughly 100-fold higher than those used in earlier SM studies are employed such that spatial variations in ε are readily observed. Convergence of this "quasi-SM" approach with the distributions of ε measured in true SM studies is demonstrated. For PMMA, a Gaussian distribution of ε is observed, with the mean of this distribution consistent with literature values. In PVDF, three distinct optically excited populations are observed corresponding to separate dielectric environments within the polymer. In addition, the distribution of ε measured in PVDF spans an order of magnitude. Spatially resolved (~250 nm) images of ε in PMMA and PVDF obtained in the quasi-SM studies are also presented, with PMMA demonstrating fewer environments with smoother boundaries in comparison to PVDF, which demonstrates spatial variation in ε. In summary, the results presented here demonstrate that quasi-SM confocal microscopy provides a simple and direct way to measure distributions of ε in polymer films with nanometer lateral resolution.

EXPERIMENTAL SECTION

Sample Preparation. *PMMA Films.* Nile Red (NR, Aldrich, powder, 99+% pure by LC−MS) was used as received. A 3.5×10^{-5} M NR solution and a 10 wt % poly(methyl methacrylate) (PMMA, Sigma Aldrich, MW ≈ 15 000 by GPC) solution in toluene (Fisher Scientific, HPLC grade) were prepared. Aliquots of the NR stock solution were then added to the polymer solution to produce final NR concentrations of 10^{-7} and 10^{-9} M in 10 wt % PMMA/toluene corresponding to quasi-single molecule and single molecule samples, respectively. Glass coverslips were cleaned by boiling in a solution of 3:2:1 nanopure water (Barnstead, NANOpure II):ammonium hydroxide:hydrogen peroxide for 2 h, cooled, rinsed with nanopure water, and rapidly dried with nitrogen gas. PMMA films were prepared by spin coating coverslips at 3000 rpm for 60 s. The samples were then dried under vacuum for 30 min. Film thicknesses of 390 ± 10 nm were determined by ellipsometry (J.A Woollam Co., Inc., M-2000).

PVDF Films. A 3.1×10^{-5} M NR and a 5 wt % poly(vinylidene fluoride) (PVDF, Sigma Aldrich, MW ≈ 534 000 by GPC) solution were prepared in dimethyl sulfoxide (DMSO, EMD Chemicals Inc., ACS grade). PVDF films were prepared as the PMMA films described above except that to maximize the amount of β-phase present in the PVDF films the NR in 5 wt % PVDF/DMSO solutions were heated to 90 °C, and then spun onto clean glass coverslips at room temperature for 60 s at 1000 rpm. The films were then dried at room temperature for 1 h and in a 60 °C oven for 15 min. The resulting films thicknesses were 290 ± 10 nm as measured by ellipsometry. Films were confirmed to be in the β-phase through X-ray diffraction (Bruker AXS, D8 Discover w/ GADDS) with a diffraction peak at $2\theta = 20.8°$, confirming that maximum percentage (60%) of PVDF exists in the β-phase in agreement with the literature.[16]

Ensemble Spectroscopy. Fluorescence spectra of NR in solutions and in polymer films were acquired using 488-nm excitation (Horiba Fluorolog 3) for both polymers, and also with 579-nm excitation for PVDF. UV−Vis absorption spectra of the samples were also measured (Varian Cary Eclipse 5000). Heavily dyed films of NR in PMMA and PVDF were prepared by drop casting a ~10^{-5} M NR sample at room temperature resulting in faintly colored films. Solution-phase fluorescence spectra of ~10^{-6} M solutions of NR dissolved in hexane (Sigma Aldrich, >95%), heptane (Fisher Scientific, HPLC grade), cyclohexane (EMD, OmniSolv), toluene, chloroform (Fisher Scientific, HPLC grade), dichloromethane (EMD, HPLC grade), acetone (Sigma Aldrich, HPLC grade), and acetonitrile (EMD, HPLC grade) were collected.

Confocal Microscopy. Confocal microscopy studies were performed by placing the sample on a piezoelectric nanopositioning stage (Queensgate, NPS-XY-100B). Excitation at 488 nm (Novalux, Protera) with a power of 3 μW as measured at the entrance port of the microscope was employed. The polarization of the 488-nm excitation field was defined using a 488-nm polarizing beam splitter and converted to circular polarization using a 488-nm $\lambda/4$ waveplate. The excitation field was directed into a 1.3 NA objective (Nikon, Plan-Fluor) using a 488-nm dichroic long-pass filter. Emission was collected in an epi-geometry, the excitation field rejected using a 500 nm long-pass filter (Chroma, HQ500LP), and the emission was focused onto a pinhole (CVI, 75-μm diameter) to provide confocal resolution. The emission was split by a 600 nm short-pass dichroic mirror, with the reflected and transmitted intensity focused onto two separate avalanche photodiode detectors (Perkin-Elmer SPCM-AQR-16). Ten 10 μm × 10 μm fluorescence intensity images were collected employing a step size of 0.1 μm and an integration time of 0.2 s per step. In the single-molecule studies, ~10 individual molecules were detected per scan, resulting in a total of ~100 molecules for the total SM data set.

All data processing was performed in Matlab (version R2012b). Single NR molecules were identified using an emissive threshold defined as the average of the brightest pixel recorded by each detector in three scans of dye free

dx.doi.org/10.1021/jp4008398 | J. Phys. Chem. B XXXX, XXX, XXX−XXX

polymer films (500 and 1000 counts, for PMMA and PVDF, respectively). Images were processed by first assigning pixel values less than or equal to the threshold a null value (NaN), and the ratios of the reflected and transmitted intensities (R/T) were determined for each pixel. The remaining real-valued pixels were compiled into an array containing the data from all 10 scans, with each pixel corresponding to an element in this array. This process was repeated for the 10^{-7} M films, but without employing an emissive threshold. A mapping of the R/T ratio to emission wavelength maxima was performed by convolving ensemble NR emission spectra in hexane, toluene, and acetonitrile with the APD efficiency curves, the emission filter transmission curve, and the 600 nm dichroic reflectance and transmission curves to calculate the expected reflected (R) and transmitted (T) spectra as described previously.[17] A mapping of the R/T ratio to NR emission maximum was performed by numerically shifting the NR emission spectrum in the solvents listed above and calculating R/T. The curves that resulted were then combined to produce a "hybrid" curve that continually transforms the R/T ratio to wavelength. This incorporates the change in fluorescence line shape as the polarity of the solvent increases (see the Supporting Information). The calculated relationship between R/T and emission maximum was experimentally verified by measuring R/T values from within droplets of NR solutions on the microscope employing each solvent identified above.

RESULTS AND DISCUSSION

The studies outlined here employ NR emission solvatochromism to determine the distribution of ε in PMMA and PVDF. At room temperature, PMMA exists in a single phase and is thus expected to demonstrate a single distribution of ε with variation between local environments providing width to this distribution. Literature values for ensemble measurements of ε in PMMA are 3.0 ± 0.6.[9,14] In contrast, PVDF exists as a mixture of two dominant phases (α and β), each of which can be preferentially expressed through processing conditions. The α-phase is monoclinic and has a trans−gauche−trans−gauche (TGTG) chain conformation. The β-phase of PVDF exhibits ferroelectric behavior useful in piezoelectric and pyroelectric applications. This phase is orthorhombic with an all-trans chain conformation.[18] PVDF in the α-phase exhibits a dielectric constant of $\varepsilon = 6$, increasing to 13 with an increase in the amount of β-phase.[12] In our studies, processing conditions described above were chosen to maximize the percentage of β-phase to produce a broad range of dielectric constants.

Ensemble absorption and emission spectra of NR in PVDF and PMMA films are presented in Figure 2. For NR in PMMA, a Stokes shift of ∼40 nm is observed with absorption and emission demonstrating similar line shapes. In contrast, for NR in PVDF, the line shapes for absorption and emission are significantly different. Computational studies of NR assign the absorption of NR to an electronic transition between a single ground (S_0) and locally excited (LE) state; therefore, the multiple peaks evident in the absorbance spectrum of NR in PVDF suggest that there are subpopulations of NR in different dielectric environments.[11] With regards to the emission spectrum, previous observations of "dual-emission" or multiple emission peaks for NR have been attributed to emission from both locally excited (LE) and twisted intramolecular charge transfer (TICT) states.[9,19−21] The TICT excited state is formed via intramolecular charge transfer from the LE state through rotation of the amine group. Population of the TICT excited

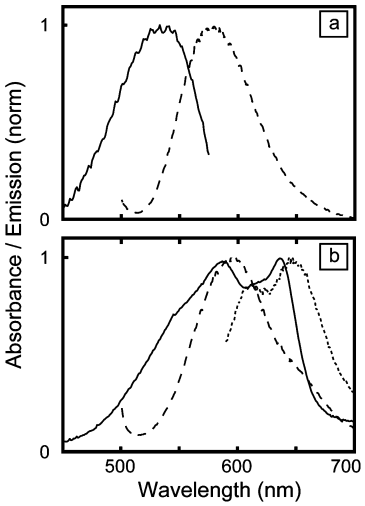

Figure 2. Absorbance (−) and emission (− − −) spectra for (a) NR in PMMA with 488-nm excitation. Band maxima occur at λ_{abs} = 533 nm and λ_{fluor} = 579 nm. (b) NR in PVDF with a 488-nm excitation (− − −) and 579-nm excitation (- - -). Band maxima occur at λ_{abs} = 550, 587, and 636 nm, while λ_{fluor} = 600 and 650 nm for NR in PVDF.

state occurs in polar, protic solvents where hydrogen bonds stabilize the TICT excited state, and the energy of the TICT state is lower relative to the LE state. The fluorescence quantum yield for NR in alcohols is diminished relative to nonpolar solvents, and the shift in emission maximum follows a different relationship with dielectric constant than is seen with polar aprotic solvents.[10] Because PVDF is polar and aprotic, we expect the NR emission to be dominated by LE state emission such that Figure 2 is interpreted as reflecting NR emission from different dielectric environments. Previous evidence for NR existing in different dielectric environments was found in studies of NR dual emission in polystyrene films.[21] To test the dielectric-subpopulation hypothesis, the excitation wavelength was changed from 488 to 579 nm, which resulted in enhanced emission at longer wavelengths (Figure 2) consistent with the emission arising from subpopulations of NR in different dielectric environments.

In quasi-SM studies, 10^{-7} M NR concentrations were used to measure the dielectric heterogeneity of the polymer films. This concentration is roughly 100 times greater than that used in true SM studies, corresponding to a luminophore number density ∼10 molecules/μm^2. When compared to the spatial resolution of the microscope (∼0.250 μm), this concentration should result (on average) in two molecules being present in the illuminated volume. Figure 3 presents a 10 × 10 μm image of the NR emission maxima in PMMA and PVDF films obtained by measuring the reflected and transmitted emission intensities from a 600-nm dichroic mirror. Differences between reflected and transmitted intensity provide a measure of the NR emission maximum as a function of position. Spatial variation in the NR emission maximum is evident in both films corresponding to a spatial variation in ε in the polymer films. Comparison of the two images reveals that PVDF demonstrates a greater variation in ε relative to PMMA. This difference is further evidenced by the plot of emission wavelength versus distance for a line profile across the images as shown in Figure 3c and d. The PVDF film exhibits domains of different emission wavelengths including the "blue" and "red" emitting domains (550 and 650 nm, respectively) in addition to the dominant

dx.doi.org/10.1021/jp4008398 | J. Phys. Chem. B XXXX, XXX, XXX−XXX

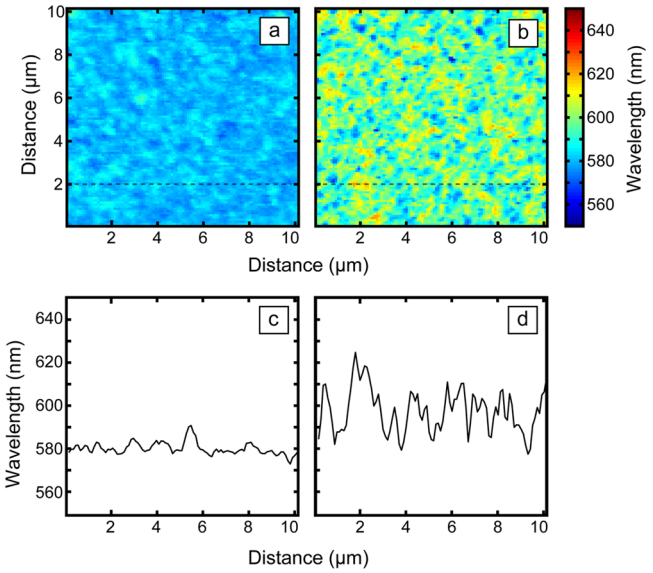

Figure 3. 10 × 10 μm images of 10^{-7} M NR in ~400 and ~300 nm thick films of (a) PMMA and (b) PVDF, respectively. Images correspond to the variation in NR emission maximum versus position in the film. Data were collected by separating the emission using a 600-nm short pass mirror and detecting the reflected and transmitted intensity using separate APDs. The ratio of the intensities for a specific location is calculated and transformed into wavelength as described in the text. Dashed line in (a) corresponds to the line plot shown in (c) demonstrating the relatively modest spatial variation in ε in PMMA. In contrast, the dashed line in (b) corresponds to the line plot shown in (d) where substantial spatial variation in ε is observed in PVDF.

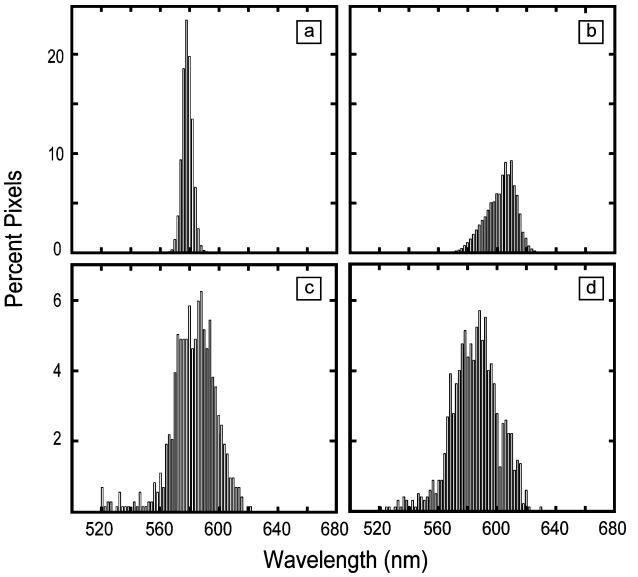

Figure 4. NR emission wavelength histograms obtained in quasi-single molecule (10^{-7} M) and true-single molecule (10^{-9} M) studies: (a) 10^{-7} M NR in PMMA, (b) 10^{-7} M NR in PVDF, (c) 10^{-9} M NR in PMMA, and (d) 10^{-9} M NR in PVDF. All histograms were compiled from 10 scans each, which allowed for the inclusion of ~100 molecule's data into the single molecule histograms.

domain corresponding to the "green" (600 nm) domains. This result suggests that PVDF films are characterized by multiple dielectric environments supporting the interpretation of the ensemble absorbance and emission spectra presented earlier. The images shown in Figure 3 provide a direct measure of the degree of spatial variation in ε for the polymer films. For example, the line scan provided in Figure 3d reveals a region of red-shifted NR emission in PVDF centered at ~2 μm with a full width half max of ~1 μm. The direct measurement of spatial variation in ε is a unique capability of this technique, with lower concentration studies lacking the NR number density to compare neighboring regions in the films.

Convergence of quasi and true SM measured ε distributions is demonstrated in Figure 4. The figure presents histograms of emission maxima for the 10^{-7} M (quasi) and 10^{-9} M (true SM) NR films. Both techniques demonstrate that the distribution of emission maxima is narrower for PMMA in comparison to PVDF, consistent with a greater distribution of ε in PVDF. Distributions of emission maxima obtained in the SM studies (bottom panels of Figure 4) are in very good agreement with the quasi-SM results, with differences reflecting the limited emission statistics available in the SM studies. In terms of distribution averages, the single molecule data have an average emission wavelength in PMMA of $\lambda_{average}$ = 583 nm (quasi λ_{max} = 580 nm) and 586 nm in PVDF (quasi λ_{max} = 603 nm).

The quasi-SM technique relies on correlation between the NR emission maxima and ε. This correlation has been previously quantified using the spectral shift in NR emission in condensed environments relative to the vapor phase:[12]

$$\Delta E_F = E_F - E_F{}^0 = c_1\frac{n^2-1}{2n^2+1} + c_2\left(\frac{\varepsilon-1}{\varepsilon+2} - \frac{n^2-1}{n^2+2}\right)$$

In the above expression, E_F is the measured NR emission maximum in eV, $E_F{}^0$ is the vapor phase emission maximum, n is the index of refraction, ε is the dielectric constant, and c_1 = −1.128 eV and c_2 = −0.556 eV are empirical constants. Although the equation above is in qualitative agreement with the solvatochromic shifts exhibited by NR (Figure 1), the model does not accurately capture the relationship between ε and emission maximum at values of ε less than 5 and greater than 10. The connection between NR's solvatochromism and ε was central to the previous work of Higgins and co-workers.[9] In their paper, the NR emission energy is given by $\bar{\nu}_{fl} = \Delta G^\circ - \lambda_0 - \lambda_i$, where λ_0 is the solvent reorganization energy and λ_i is the internal molecular reorganization energy of the solute. The solvent reorganization energy was modeled as a dielectric continuum such that:

$$\lambda_0 = \frac{(\Delta\mu)^2}{hca^3}\left[\frac{\varepsilon-1}{2\varepsilon+1} - \frac{\eta^2-1}{2\eta^2+1}\right]$$

In the above expression, ε is the static dielectric constant, η^2 is the optical dielectric constant (index of refraction), a is the radius of the spherical cavity in which the solute resides, h is Planck's constant, c is the speed of light, and $\Delta\mu$ is the change in dipole moment between the ground and excited states. Next, λ_0 can be separated into static and dynamic components, denoted as λ_{00} and λ_{0i}, respectively. In this approach, λ_{0i} represents the contribution to the reorganization energy from solvent relaxation during excited state lifetime (i.e., vibrational relaxation), denoted as a dynamic dielectric constant, ε_{dyn}, and in general $\varepsilon > \varepsilon_{dyn}$ due to ε_{dyn} corresponding to solvent dynamics on the ~2 ns time scale. Using the following substitution $f(D) = ((D-1)/(2D+1))$, the solvent reorganization energy becomes:[22]

dx.doi.org/10.1021/jp4008398 | J. Phys. Chem. B XXXX, XXX, XXX−XXX

$$\lambda_0 = \lambda_{0i} + \lambda_{00}$$

$$\lambda_{00} = \frac{(\Delta\mu)^2}{hca^3}(f(\varepsilon) - f(\varepsilon_{dyn}))$$

$$\lambda_{0i} = \frac{(\Delta\mu)^2}{hca^3}(f(\varepsilon_{dyn}) - f(\eta^2))$$

Finally, Higgins identifies the part of ΔG° that gives rise to emission energy shifts relative to the vapor phase as $\Delta\Delta G$:

$$\Delta G^\circ = \Delta G_v - \Delta\Delta G \quad \text{and} \quad \Delta\Delta G = \frac{\Delta(\mu^2)}{hca^3}\left[\frac{\varepsilon - 1}{2\varepsilon + 1}\right]$$

In the above expression, $\Delta(\mu^2) = (\mu_e{}^2 - \mu_g{}^2)$, with subscripts e and g denoting the excited- and ground-state permanent dipole moments, respectively. The above expressions allow one to estimate the contributions from λ_{0i} and $\Delta\Delta G$ to the solvatochromic shift in NR emission. Using reasonable parameters for NR[9,23] in PMMA (μ_g of 11 D, $\Delta\mu$ of 5 D, a = 5 Å, η = 1.4), we find that for ε and ε_{dyn} = 2, $\lambda_{0i} \approx 10$ cm^{-1} and $\Delta\Delta G \approx 1000$ cm^{-1}; and for ε and ε_{dyn} = 5, $\lambda_{0i} \approx 150$ cm^{-1} and $\Delta\Delta G \approx 2000$ cm^{-1}. In short, these estimates demonstrate that the solvatochromic shift exhibited by NR is dominated by $\Delta\Delta G$, and this quantity is directly related to ε.

The empirical relationship between NR emission max and ε was established by measuring the NR emission energies in various solvents of known ε as shown in Figure 5. For completeness, the variation in NR emission maximum with solvent $E_T(30)$ value is also shown.[24] The figure demonstrates that small variations in dielectric constant result in large shifts in emission energy when ε < 5, but only modest shifts in emission are observed when ε > 10. The solvochromatic shift of NR with ε was best fit by a sum of two exponentials: $E_F(\varepsilon) = A\ e^{-B\varepsilon} + C\ e^{-D\varepsilon}$, with best fit corresponding to $A = (1.076 \pm 1.179) \times 10^4$, $B = 0.8 \pm 0.6$, $C = (1.67 \pm 0.05) \times 10^4$, and $D = 0.0005 \pm 0.001$. Using this equation, the maximum of emission wavelength distributions for PMMA and PVDF from Figure 4a,b (580 and 596 nm, respectively) corresponds to ε = 3.64 for PMMA and ε = 10.72 for PVDF, in good agreement with ensemble measurements.[14] This conversion is further illustrated through the transformation of the spatially mapped emission wavelength maximum to ε for the scans in Figure 3 as shown in Figure 6. The best fit used to transform the distribution of E_F to distributions of ε is also shown in Figure 7. The quasi-SM

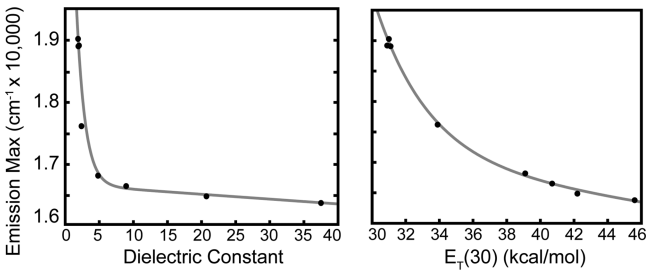

Figure 5. (a) NR fluorescence emission maximum versus ε. Data are fit to a sum of two exponentials (gray line) of the form $E_{max} = A\ e^{-B\varepsilon} + C\ e^{-D\varepsilon}$ with best-fit parameters $A = (1.076 \pm 1.179) \times 10^4$, $B = 0.8 \pm 0.6$, $C = (1.67 \pm 0.05) \times 10^4$, and $D = 0.0005 \pm 0.001$. (b) NR emission maximum versus solvent $E_T(30)$ values. Best fit to a sum of two exponentials is shown (gray line), with best-fit parameters $A = (3 \pm 20) \times 10^7$, $B = 0.3 \pm 0.25$, $C = (1.8 \pm 0.4) \times 10^4$, and $D = 0.003 \pm 0.005$.

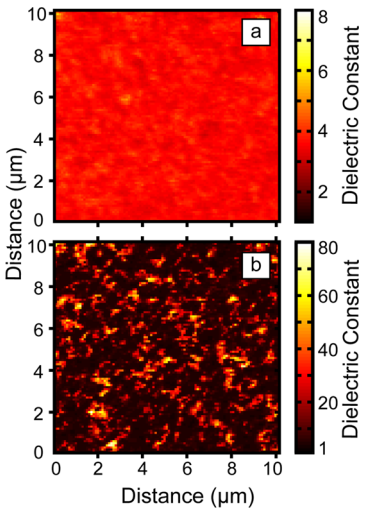

Figure 6. 10 × 10 μm images depicting the spatial distribution in ε for the same scans as in Figure 3. Images correspond to the polymer's dielectric constant versus position in the film. Note the order of magnitude difference in the color bar scale between (a) and (b).

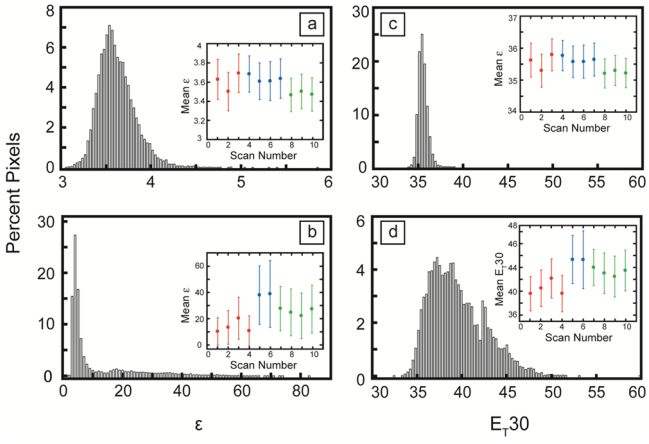

Figure 7. Histograms representing the distribution of ε and $E_T(30)$ values from the 10 × 10 μm scans in Figure 3. Shown are dielectric distributions in (a) PMMA (ε_{mean} = 3.64 ± 0.21, ε_{mode} = 3.55) and (b) PVDF (ε_{mean} = 10.72, ε_{mode} = 16.99). Also shown are distributions of $E_T(30)$ values in (c) PMMA (mean = 35.64 ± 0.51) and (d) PVDF (mean = 39.61 ± 3.05). Each histogram is comprised of 100 bins. The insets in (a)–(d) show the mean value of ε determined for 10 individual scans (error bars: one standard deviation). The data of the same color represent adjacent areas, while the distances between red, blue, and green regions are ~1 mm.

PMMA film demonstrates a Gaussian distribution of dielectric constants with a maximum at ε = 3.64 and standard deviation of 0.21. The corresponding histogram for PVDF is a heavy tailed distribution with values of ε spanning an order of magnitude. A component of the distribution tailing toward higher ε arises from the modest change in NR emission when ε > 10 noted earlier. However, this tailing is not due exclusively to this effect as the observation of high-ε domains in PVDF is not unreasonable. Specifically, the ensemble emission spectra demonstrate a shoulder at 650 nm (1.54×10^4 cm^{-1}) consistent with ε > 40, demonstrating that high-dielectric environments are present. Figure 7b demonstrates that environments for which 40 < ε < 80 are not very probable, and comprise only 5% of the distribution. A second result in

dx.doi.org/10.1021/jp4008398 | J. Phys. Chem. B XXXX, XXX, XXX–XXX

PVDF is that the ε distributions vary significantly between different regions of the film. The inset in Figure 7b presents a plot of the mean ε calculated for 10 individual scans with the error bars representing one standard deviation. This plot demonstrates the substantial variation in both the mean and the width of the ε distribution in different regions of the PVDF film. This result validates the importance of investigating relatively large regions of polymer films to get a true sense of the total variation of ε, an investigation that is easily done using the quasi-SM technique. In comparison, a single 10×10 μm region of PMMA (Figure 7a, inset) captures the full extent of the variation of ε, with the mean value of ε for 10 scans (taken from different regions of the film) falling within the standard deviation of a single scan. This result demonstrates that for PMMA, variations in ε only occur on submicrometer length scales.

Given the limited variation in NR emission energy at higher ε, we explored an alternate method of characterizing the polymer environment in terms of $E_T(30)$ values.[25] Figure 5b presents the NR emission maximum versus $E_T(30)$ for the solvents studied.[24,26] The variation in emission maximum with $E_T(30)$ was best fit to a sum of two exponentials with best fit corresponding to $A = (3 \pm 20) \times 10^7$, $B = 0.3 \pm 0.25$, $C = (1.8 \pm 0.4) \times 10^4$, and $D = 0.003 \pm 0.005$. The figure demonstrates that greater variation in the NR emission maximum at higher $E_T(30)$ is observed in comparison to the dependence on ε described above. Similar findings have been reported by Deye et al.[27] Using the best fit, the distribution of $E_T(30)$ values in both PMMA and PVDF was determined as shown in Figure 7. Similar to dielectric constant, the distribution of $E_T(30)$ in PMMA is narrow, and becomes significantly broader in PVDF, which exhibits a right skew in the distribution indicating the presence of regions with considerable polarity.

CONCLUSION

The results presented here demonstrate that quasi-SM microscopy can be used to measure both the distribution and the spatial variation in dielectric environments in polymer films from submicrometer to millimeters. As compared to previous techniques employed to measure the dielectric constant of polymers, this approach is flexible, efficient, and allows for the measurement of the spatial variation in dielectric constant. Using this approach, the variation of ε in films of PMMA and PVDF was determined. PMMA exhibited a narrow distribution of dielectric environments, while the corresponding distribution in PVDF is much broader. Perhaps the most intriguing capability of the quasi-SM measurements is the ability to map out the spatial variation of ε in the polymer films (Figure 6a and b). Time-resolved applications of this technique could be used to provide information on the time and length scales for the interchange of dielectric environments in polymer films, information that would be critical in testing current models of dynamic heterogeneity in polymers.[28−30] In summary, quasi-SM confocal microscopy provides a novel approach to classifying and studying the dielectric environments of polymer films.

ASSOCIATED CONTENT

Supporting Information

Figure S1: Plots representing the method used to transform R/T to emission wavelength max. (a) APD efficiency curve (red), emission filter transmission curve (blue), and 600-nm dichroic reflectance (purple) and transmission (green) curves used to calculate the expected reflected and transmitted spectra. (b) Curves representing the relationship between emission wavelength and R/T values as obtained from shifting the bulk fluorescence spectrum of hexane (dark blue □), toluene (green ○), and acetonitrile (red △) and convolving with the curves presented in (a). "●" represent the "hybrid" curve, constructed by weighing the variation in NR emission line shape with a change in solvent polarity, used to accurately transform R/T to wavelength. Blue "◆" represent the R/T values measured for NR solutions on the microscope for verification of the "hybrid" curve's accuracy. This material is available free of charge via the Internet at http://pubs.acs.org.

AUTHOR INFORMATION

Corresponding Author

*E-mail: pjreid@uw.edu.

Notes

The authors declare no competing financial interest.

ACKNOWLEDGMENTS

This work was supported by the National Science Foundation (DMR 1005819). Part of this work was conducted at the University of Washington NanoTech User Facility, a member of the NSF National Nanotechnology Infrastructure Network (NNIN). E.A.R. was supported in part by the UW NIEHS-sponsored Biostatistics, Epidemiologic and Bioinformatic Training in Environmental Health (BEBTEH) Training Grant, Grant no.: NIEHS T32ES015459.

REFERENCES

(1) Fumagalli, L.; Ferrari, G.; Sampietro, M.; Gomila, G. *Nano Lett.* **2009**, *9*, 1604−1608.
(2) Riedel, C.; Arinero, R.; Tordjeman, P.; Lévêque, G.; Schwartz, G. A.; Alegria, A.; Colmenero, J. *Phys. Rev. E* **2010**, *81*, 010801.
(3) Riedel, C.; Sweeney, R.; Israeloff, N. E.; Arinero, R.; Schwartz, G. A.; Alegria, A.; Tordjeman, P.; Colmenero, J. *Appl. Phys. Lett.* **2010**, *96*, 213110.
(4) Bale, D. H.; Eichinger, B. E.; Liang, W. K.; Li, X. S.; Dalton, L. R.; Robinson, B. H.; Reid, P. J. *J. Phys. Chem. B* **2011**, *115*, 3505−3513.
(5) Serghei, A.; Tress, M.; Kremer, F. *Macromolecules* **2006**, *39*, 9385−9387.
(6) Crider, P. S.; Majewski, M. R.; Zhang, J.; Oukris, H.; Israeloff, N. E. *Appl. Phys. Lett.* **2007**, *91*, 013102.
(7) Greenspan, P.; Fowler, S. D. *J. Lipid Res.* **1985**, *26*, 781−789.
(8) Levitsky, I.; Krivoshlykov, S. G.; Grate, J. W. *Anal. Chem.* **2001**, *73*, 3441−3448.
(9) Hou, Y. W.; Bardo, A. M.; Martinez, C.; Higgins, D. A. *J. Phys. Chem. B* **2000**, *104*, 212−219.
(10) Rei, A.; Ferreira, M. I. C.; Hungerford, G. *J. Fluoresc.* **2008**, *18*, 1083−1091.
(11) Freidzon, A. Y.; Safonov, A. A.; Bagaturyants, A. A.; Alfimov, M. V. *Int. J. Quantum Chem.* **2012**, *112*, 3059−3067.
(12) Martins, P.; Serrado Nunes, J.; Hungerford, G.; Miranda, D.; Ferreira, A.; Sencadas, V.; Lanceros-Méndez, S. *Phys. Lett. A* **2009**, *373*, 177−180.
(13) Gross, S.; Camozzo, D.; Di Noto, V.; Armelao, L.; Tondello, E. *Eur. Polym. J.* **2007**, *43*, 673−696.
(14) Brandrup, J.; H., I. E.; Grulke, E. A.; Akihiro, A.; Bloch, D. R. *Polymer Handbook*; Wiley: New York, 1999.
(15) Ameduri, B. *Chem. Rev.* **2009**, *109*, 6632−6686.
(16) Satapathy, S.; Pawar, S.; Gupta, P. K.; Varma, K. B. R. *Bull. Mater. Sci.* **2011**, *34*, 727−733.
(17) Riley, E. A.; Hess, C. M.; Pioquinto, J. R. L.; Kaminsky, W.; Kahr, B.; Reid, P. J. *J. Phys. Chem. B* **2012**, *117*, 4313−4324.
(18) Lovinger, A. J. *Developments in Crystalline Polymers*; Applied Science Publishers Ltd.: England, 1982; Vol. *1*.

(19) Dutta, A. K.; Kamada, K.; Ohta, K. *J. Photochem. Photobiol., A* **1996**, *93*, 57−64.
(20) Jee, A. Y.; Park, S.; Kwon, H.; Lee, M. *Chem. Phys. Lett.* **2009**, *477*, 112−115.
(21) Kim, H. H.; Song, N. W.; Park, T. S.; Yoon, M. *Chem. Phys. Lett.* **2006**, *432*, 200−204.
(22) Marcus, R. A. *J. Phys. Chem.* **1990**, *94*, 4963−4966.
(23) Kawski, A.; Bojarski, P.; Kuklinski, B. *Chem. Phys. Lett.* **2008**, *463*, 410−412.
(24) Reichardt, C. *Chem. Rev.* **1994**, *94*, 2319−2358.
(25) Rauf, M. A.; Soliman, A. A.; Khattab, M. *Chem. Cent. J.* **2008**, *2*, 19.
(26) Deng, Q.; Li, Y.; Wu, J.; Liu, Y.; Fang, G.; Wang, S.; Zhang, Y. *Chem. Commun.* **2012**, *48*, 3009−3011.
(27) Deye, J. F.; Berger, T. A.; Anderson, A. G. *Anal. Chem.* **1990**, *62*, 615−622.
(28) Gebremichael, Y.; Schróder, T. B.; Starr, F. W.; Glotzer, S. C. *Phys. Rev. E* **2001**, *64*, 051503.
(29) Ediger, M. D. *Annu. Rev. Phys. Chem.* **2000**, *51*, 99−128.
(30) Wolynes, P. G. *Proc. Natl. Acad. Sci. U.S.A.* **2009**, *106*, 1353−1358.